UCLA

Structural & Geotechnical Engineering Laboratory

CPT-BASED ULTRASONIC PROBE FOR P-WAVE REFLECTION IMAGING OF EMBEDDED OBJECTS

Scott J. Brandenberg

Joseph Coe

University of California, Los Angeles
Department of Civil & Environmental Engineering

UCLA - SGEL
Report 2010/01

FUNDING AGENCY ACKNOWLEDGMENT AND DISCLAIMER

Funding for this work was provided by UCLA and by Caltrans under contract number 59A0691.

The contents of this report reflect the views of the authors who are responsible for the facts and accuracy of the data presented herein. The contents do not necessarily reflect the official views or policies of the State of California or the Federal Highway Administration. This report does not constitute a standard, specification, or regulation.

CPT-BASED ULTRASONIC PROBE FOR P-WAVE REFLECTION IMAGING OF EMBEDDED OBJECTS

Scott J. Brandenberg[1] and Joseph Coe[2]

Abstract: An ultrasonic p-wave reflection imaging probe is developed and utilized to non-invasively image the geometry of a deep foundation supporting a bridge pier. The source ultrasonic transducer emits compressive waves into saturated soil that subsequently transmit to and reflect back from an embedded object, and the receiver transducer measures the reflections which are used to construct an image. The components of the system, including the custom transducer probe and data acquisition hardware, were integrated with the *nees@UCLA* cone penetration testing (CPT) truck. The transducers have a central frequency of 100kHz, and have a diameter-to-wavelength ratio of more than 3 in soft saturated soils with p-wave velocities similar to water (i.e., 1500m/s). The large diameter-to-wavelength ratio gives the transducers a directivity pattern that controls the rate at which wave amplitude attenuates with distance. The transducers are impedance matched to water, and are therefore reasonably efficient transmitters in saturated soil, but inefficient in unsaturated soil. The probe was utilized to successfully image a pile foundation in very soft saturated clay, but returns were not recorded in stiffer and/or unsaturated soils. Causes of the poor returns include the scattering effects of large soil particles, coupling between the transducers and the soil, and drift of the probe out of alignment with the pile foundation. The probe could be very useful for non-destructive quality assurance of structural elements constructed in-situ in soft saturated soils,

[1] Assistant Professor, 5731 Boelter Hall, Department of Civil and Environmental Engineering, University of California, Los Angeles, CA 90095-1593, email: sjbrandenberg@ucla.edu
[2] Assistant Professor, 301 Letellier Hall, Department of Civil and Environmental Engineering, The Citadel, Charleston, SC, 29409, email: jcoe3@citadel.edu

and provides higher resolution measurements of the shape of the embedded object compared with other available methods.

Subject Headings: Reflection; Compression waves; Ultrasonic methods; Nondestructive testing; Integrity testing; Deep foundations; Transducers; Imaging techniques; Signal processing

Introduction

Inadequate knowledge about the subsurface is among the biggest problems in geotechnical engineering. Current standard of practice site investigation techniques can leave us with an incomplete understanding of site conditions that is often utterly inadequate to reliably perform engineering analysis (Terzaghi 1947). The standard penetration test and cone penetration test methods provide information about only a small fraction of the soil at a site, and we are left to interpolate soil properties between measured data points based on geologic history, statistical methods, and judgment. Furthermore, these methods often provide poor correlation with key soil properties (e.g., SPT is a poor indicator of undrained shear strength in soft clays), and SPT measurements can be highly operator-dependent. Site investigation is arguably the area of geotechnical engineering that is in the most need of improvement.

This problem is not unique to geotechnical engineering. Geology faced uncertainty regarding the composition of the interior of the earth since invasive investigations were cost-prohibitive and could only yield information about a limited portion of the upper crust. A basic model of the earth was constructed non-invasively based on measurements of earthquake-generated seismic waves (e.g., Mohorovičić 1910). Geophysical methods have been used extensively for non-invasively locating hydrocarbon-containing anticline features often kilometers below the earth's surface (e.g., Yilmaz 1987, Sheriff and Geldart 1995).

Geophysical methods are widely used in geotechnical engineering to measure shear wave velocity, acknowledged as an important soil property for dynamic problems such as earthquakes, construction vibrations, etc. However, wave-based imaging methods, in which waves are used to measure positions of interfaces rather than soil properties, have not been as

widely adopted. A number of hurdles have contributed to this, including the complexity and specialized nature of the work, the high cost of required equipment, and lack of exposure in typical undergraduate engineering curricula. Furthermore, many wave-based imaging techniques utilize p-waves rather than s-waves, but s-waves are typically considered more important than p-waves for geotechnical applications due to their importance in dynamic problems.

A handful of studies have been conducted to demonstrate the potential of p-wave imaging. For example, Lee and Santamarina (2005) conducted a small-scale laboratory test program that utilized 500 kHz ultrasonic transducers to image soil layers, embedded objects, and slurry surface position during sedimentation. Coe and Brandenberg (2010) also utilized ultrasonic transducers to construct 3-D images of small-scale soil models, and found that migration significantly improved image accuracy for dipping reflectors. Grandjean (2006) utilized a seismic "multi-approach" that identified contaminants in the field using a number of different types of waves, including p-waves (Rayleigh waves and shear were also utilized). Kase and Ross (2004) used reflection imaging in advance of tunnel excavation to identify potentially difficult soil conditions. Nichols et al. (1987) located rebound fracture zones in Pierre shale using shallow seismic reflection imaging. More research is necessary to adapt p-wave reflection imaging techniques from other fields to geotechnical projects both at the laboratory and field scales.

This paper presents a CPT-based ultrasonic p-wave reflection imaging system intended to image vertically-oriented embedded structural elements. A number of methods exist for detecting flaws in pile foundations, or to determine their depth. For example, Olson and Aouad (1998) summarized many different surface-based and borehole-based techniques for

measuring the length of pile foundations for the purpose of evaluating scour hazard. They found that the parallel seismic method had the broadest applicability for determining the depth of embedment of pile foundations. This method involves lowering a hydrophone into a fluid-filled cased borehole, and striking the top of the foundation with a hammer, generating a downward propagating compressive wave with a frequency in the sonic range (i.e., signals with central frequency around 250Hz were presented in their study). The compressive waves are transmitted away from the pile foundation and can be recorded by the hydrophone. When the hydrophone is lowered beneath the bottom of the pile foundation, the recorded wave amplitude becomes much smaller, thereby enabling determination of pile length. Additional methods often used for quality assurance of drilled shafts include sonic echo, cross-hole sonic logging, and gamma-gamma logging. These methods provide information of the drilled shafts typically only inside the rebar cage, where the casings are installed. The ultrasonic imaging technique presented in this report differs from existing techniques since (1) it uses higher frequency wave energy (i.e., 100 kHz compared with the sonic range), and (2) it provides the capability of imaging the outside of the foundation element.

The ultrasonic probe was integrated with the nees@UCLA CPT truck and is pushed into the soil alongside an embedded object to visualize its profile with depth. The ultrasonic transducers emit compressive waves into the soil that subsequently transmit to the foundation element, and measurements of the reflections are used to construct the images. Several considerations regarding application of ultrasound to soil is discussed first, followed by a description of the transducers and data acquisition system utilized in this study. Then the results from one successful and one unsuccessful field deployment at different sites in California are presented.

The successful deployment consisted of very soft clay, and was ideally suited to couple well with the transducers and propagate ultrasonic waves. A section of the pile foundation at this site was imaged successfully. The unsuccessful site consisted of stiff unsaturated sandy clay that was not ideally suited for use with the probe. Imaging was not successful at this site, but helped establish limits on soil conditions through which the probe can propagate waves and can be successfully pushed.

Application of Ultrasound in Soil

Several important considerations affect the ability to propagate ultrasonic waves through soils. First, high frequencies are desired to improve resolution, but high frequency waves attenuate more quickly with distance in material that exhibits damping. Hence, obtaining adequate resolution and penetration distance requires compromise that must be carefully considered. Second, ultrasonic transducers cannot be impedance-matched for every soil condition. If the acoustic impedance of the soil differs significantly from the design impedance, the amplitude of the transmitted wave will be less than optimal. This is an important consideration for soft soil, since p-wave velocity (and hence acoustic impedance) depends strongly on degree of saturation. Third, soil is dispersive for a number of reasons. Layered soil profiles are dispersive for surface waves since waves of various wavelength involve different strata and therefore propagate at different velocities. Saturated soils are dispersive due to Biot-flow-induced damping, which can affect highly-permeable soils at earthquake frequencies, or less permeable soils at higher frequencies. Additionally, large particles can scatter seismic waves, particularly when the wavelength is short relative to the particle size. For sonic waves,

wavelengths are typically very large relative to particle size, hence the soil is modeled as a continuum without explicit consideration of particle scattering. However, ultrasonic waves have much shorter wavelengths and care must be given to the wavelength-to-grain size ratio to ensure that the ultrasonic waves can be transmitted through the soil. Finally, good coupling between the transducer and soil is required so that the waves propagate through the soil-transducer interface.

Attenuation of P-waves in Soil

Selecting a central frequency for ultrasonic transducers must balance the conflicting goals of high resolution using high-frequency waves and the ability to transmit the waves a sufficient distance through heterogeneous attenuative materials. Eq. 1 quantifies attenuation of wave amplitude with distance, where r_2 and r_1 are distances to the source, A_2 and A_1 are wave amplitudes at r_2 and r_1, respectively, ζ is a geometrical damping term (0 for plane wave fronts, 0.5 for cylindrical wavefronts, and 1.0 for spherical wave fronts), ω is the angular frequency, D is the damping coefficient, V_p is p-wave velocity, and T is an apparent attenuation factor that accounts for partial transmission, mode conversion and other sources of heterogeneity (e.g., Santamarina et al. 2001). Understanding attenuation with distance an important consideration for design of an ultrasonic transducer because the reflected wave must be detectable.

$$\frac{A_1}{A_2} = \left(\frac{r_2}{r_1} \right)^{\zeta} e^{\frac{\varpi D}{V_p}(r_2 - r_1)} T^{-1} \quad (1)$$

Ultrasonic transducers do not generate spherical nor planar wave fronts, but rather exhibit a more complex directivity pattern that depends on the transducer size, shape, and central frequency, and the p-wave velocity of the medium. The directivity pattern affects ζ because geometric attenuation is specific to the transducer and medium. The directivity pattern of the transducer can be computed by assuming that every point on the transducer face is a point source that produces a spherical wavefront, based on Huygen's principle. The waves transmitted from the face of the transducer create a complex pattern of constructive and destructive interference in the near field, and a more uniform wavefield in the far-field, further away from the transducer.

Fig. 1 shows the pattern of wave amplitude for a circular transducer with diameter d=0.05m and central frequency f=100kHz propagating waves into water with V_p = 1500m/s ($k=2\pi f/V_p$ = 418.9 m^{-1}). The equation defining the pressure amplitude is shown in the figure, where A is the pressure amplitude on the face of the transducer. Also plotted in the figure is the normalized pressure amplitude versus distance along a line that runs through the center of the transducer and perpendicular to its face. The far-field attenuation is fitted with the functional form in Eq. 1 (with D=0 since damping is not considered in the equation in Fig. 1), and by regression ζ=0.57. Hence, the wave amplitude attenuates more slowly than a point source, but more quickly than a plane wave. Note that Eq. 1 does not perfectly fit the far-field data, and ζ is specific to the particular transducer/medium combination selected in the study. Furthermore, the amplitude decreases with distance from the central axis of the transducer. For transducers of any diameter and for any medium, ζ could be computed in the same fashion. In general,

transducer/media combinations with a high diameter-to-wavelength ratio will exhibit a stronger directivity pattern and smaller ζ values.

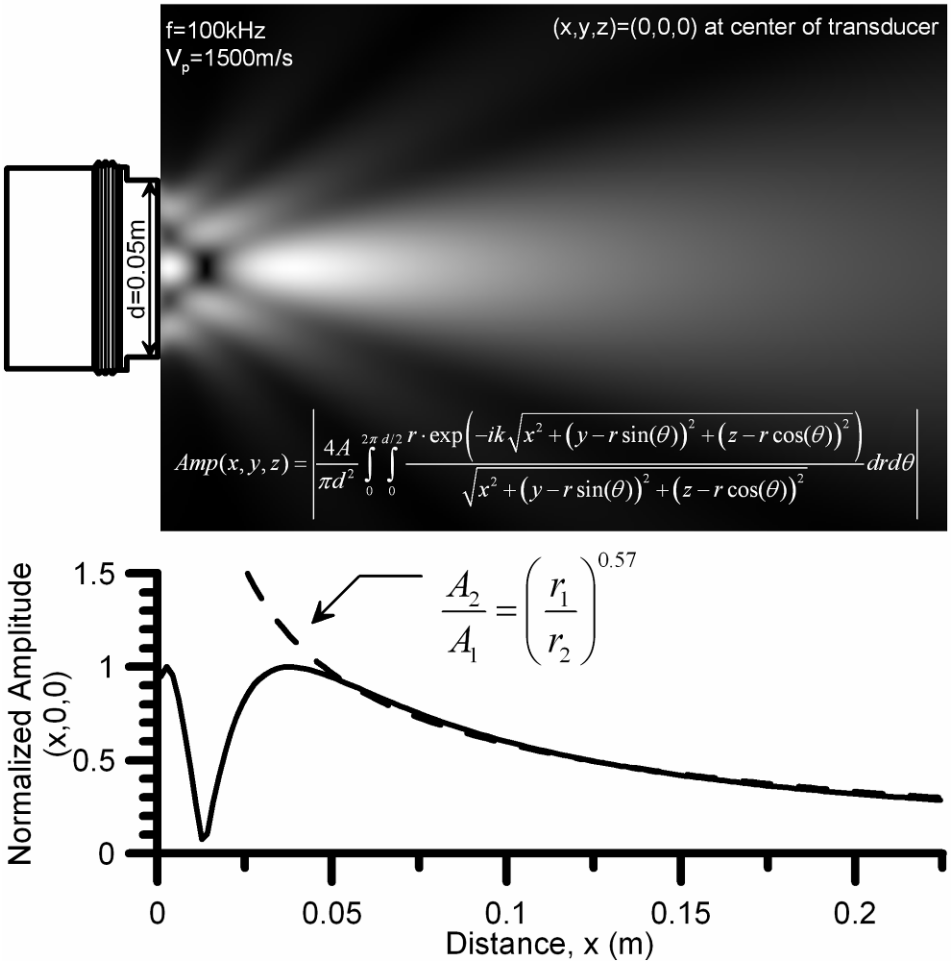

Figure 1. Transducer directivity pattern and wave amplitude as function of distance along transducer's center axis.

Small-strain damping, D, has been measured for soil using sensitive laboratory devices (e.g., Doroudian and Vucetic 1995), and typically lies in the range of 1% to 3% for slow cyclic testing. However, high-frequency waves can introduce relative inertia effects between the solid and

fluid phases in saturated soils that can increase damping due to Biot flow by 5% or more (e.g., Qiu 2010). The amount of damping depends on excitation frequency and the hydraulic conductivity of the soil, among other factors. The apparent damping parameter T is caused by transmission and reflection at normal interfaces, mode conversion of p-waves into s-waves and surface waves at inclined interfaces, and the presence of other anomalies. This damping parameter can be difficult to determine analytically since anomalies are often unknown.

Influence of Impedance Mismatch Between Soil and Transducer

P-wave velocity of soil is known to be significantly affected by degree of saturation since a small amount of compressible gas decreases bulk modulus significantly. P-wave velocity can be defined using the Gassmann equation (e.g., Santamarina 2001, Lee 2003, Lee and Santamarina 2005) as in Eq. 2, where B_{sk} is the bulk modulus of the soil skeleton, G_{sk} is the shear modulus of the soil skeleton, n is the porosity, S is the degree of saturation, B_w is the bulk modulus of water, B_a is the bulk modulus of air, B_g is the bulk modulus of the soil grains, ρ_g is the density of soil solids, and ρ_w the density of water.

$$V_P = \sqrt{\frac{\left(B_{sk} + \frac{4}{3}G_{sk}\right) + \left[n\left(\frac{S}{B_w} + \frac{1-S}{B_a}\right) + \frac{1-n}{B_g}\right]^{-1}}{(1-n)\rho_g + nS\rho_w}} \qquad (2)$$

The Gassman equation neglects differential inertial effects between the pore fluid and the solid particles that tends to increase the p-wave velocity (e.g., Biot, 1956a,b; Qiu, 2010). Nevertheless, it is a useful equation for quantifying the relation between V_p and S. Fig. 2 shows

V_p versus S for soil with various shear wave velocity values for the soil skeleton. The input parameters specified in Fig. 2 are typical for clay soil. A small amount of air in the soil matrix (i.e., S = 99%) causes a large reduction in p-wave velocity. This strong dependence is often utilized in laboratory tests wherein p-wave velocity measurements are used to verify that a high degree of saturation has been achieved. Eq. 2 assumes that the liquid and gas phases in the soil are uniformly mixed. However, Naesgaard et al. (2007) found that p-wave velocity was high in laboratory test specimens known to be unsaturated based on measurement of low B-values, and postulated that the p-wave may propagate around air bubbles through fully-saturated channels in the soil. Berge and Bonner (2002) provide further discussion of the influence of pore fluid heterogeneity, and suggest methods for distinguishing uniform versus "patchy" saturation based on p-wave and s-wave velocity measurements. Heterogeneity in the distribution of air bubbles in the void space and differential inertial effects would be expected to result in higher V_p values than predicted by Eq. 2, hence it can be considered a lower-bound estimate.

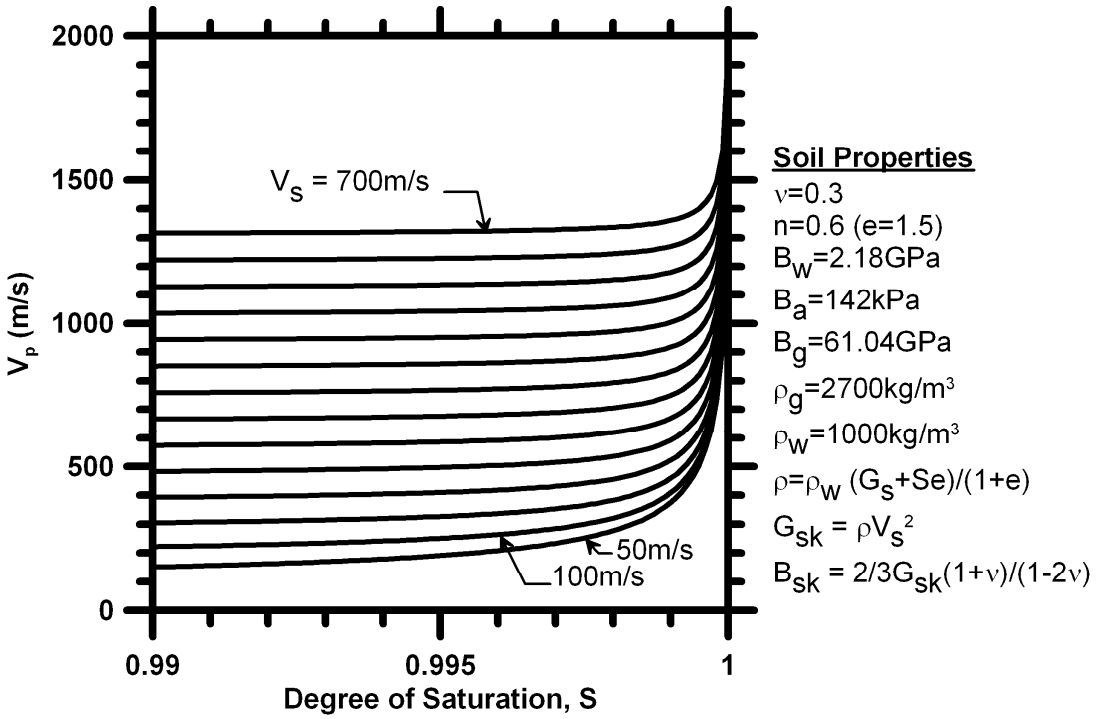

Figure 2. P-wave velocity, V_p, as function of degree of saturation based on Gassman equation.

The effect of saturation is important for ultrasonic testing because p-wave velocity affects the transmission of acoustic waves into the soil. To understand the wave amplitude transmitted into a medium by a given ultrasonic transducer, consider the schematic in Fig. 3. Ultrasonic transducers consist of a piezoelectric material that couples electrical and mechanical response, and a matching layer that acoustically matches the mechanical properties of the piezo material with the medium. Many transducers are also equipped with a backing block to reduce the pulse duration thereby improving resolution, and a replaceable delay line to prevent damage that could occur from direct contact between the transducer and the medium. The dynamic response of the transducer depends on the material properties and thicknesses of the various layers that form the transducer, the mechanical properties of the medium, and the

electrical excitation provided to the piezo material. Many researchers have developed transfer functions quantifying the transmitted pulse as a function of the electrical excitation provided to the piezo material (e.g., Leedom et al. 1971, Perrson and Hertz 1985). Such a level of detail is often required in transducer design, but a simpler model can be utilized to assess the transmission coefficient from the delay line into the medium for a given transducer.

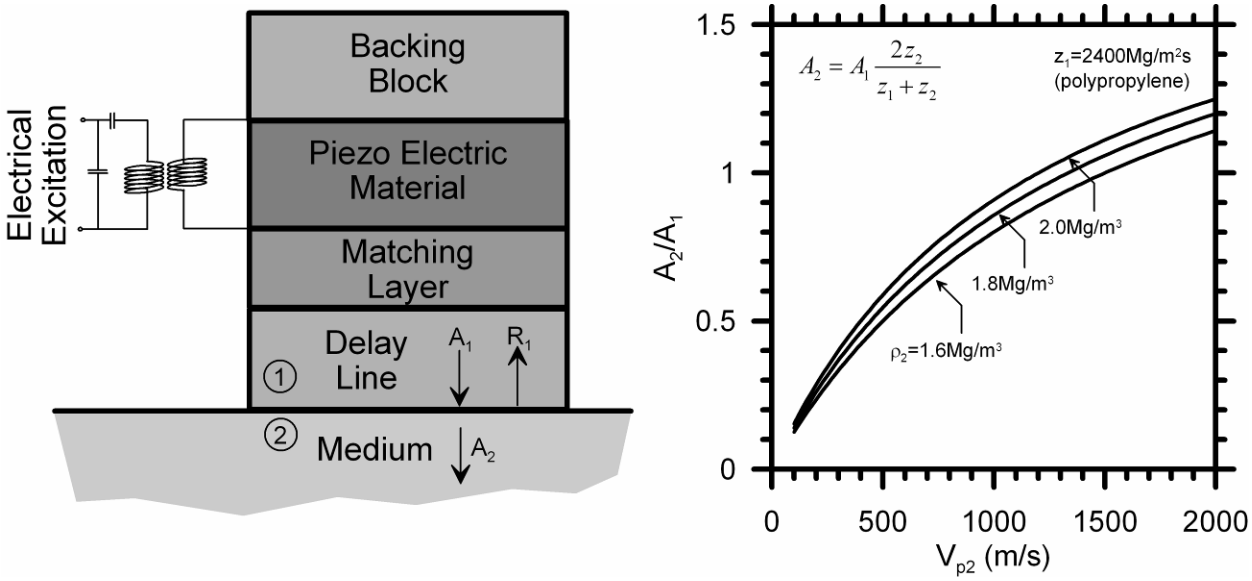

Figure 3. Transducer schematic and transmission coefficient as function of V_p in medium.

Consider a transducer with a delay line composed of polypropylene with ρ = 0.89 Mg/m^3, V_P = 2700 m/s. The acoustic impedance of the delay line is defined as z = ρV_p = 2400Mg/m^{2}s. This impedance is close to saturated clay with ρ = 1.6Mg/m^3, V_p = 1600m/s, and hence z = 2560Mg/m^{2}s. Fig. 3 presents the amplitude of the wave transmitted into the medium as a function of p-wave velocity of the medium. The transmission coefficients are plotted for several different mass densities that are characteristic of typical soils. The transmission coefficient decreases as V_p decreases. Fig. 2 shows that unsaturated soil may have V_p as low as

200m/s for reasonable V_s values, and the transmission coefficient in such cases is only about 0.2 for the polypropylene delay line. For saturated soil the transmission coefficient is closer to 1.0. Hence, this particular transducer configuration is much less efficient in unsaturated soil as in saturated soil.

P-waves in Particulate Media

Geophysical methods may assume continuum behavior for body waves where the wavelengths are very large relative to the size of the soil particles. High frequency ultrasonic waves have short wavelengths that can approach the internal scale of the soil particles, hence it is important to consider soil as a particulate material to understand limitations on its ability to propagate ultrasonic waves. Propagation of waves in soil can be understood by analogy with propagation of waves in a one-dimensional lattice of particles with lumped masses connected by elastic springs and each separated by a constant distance. Brillouin (1946) illustrated that such a lattice of particles acts as a low-pass filter because it cannot transmit waves with a wavelength smaller than twice the particle spacing. Santamarina et al. (2001) demonstrated that the Brillouin effect causes soil to become dispersive when the wavelength becomes shorter than approximately 20 times the internal scale of the particulate medium. Interparticle spacing in a lattice is analogous to particle size for soils, which establishes that soil of a given particle size can only transmit waves that are longer than some threshold wavelength. Grain size scattering will result if the wavelength becomes too small relative to the particle size. The lattice analogy is not a perfect indicator of soil behavior since soil particles exhibit a range of grain sizes and shapes, complex interparticle contacts, and often contains solid, liquid and

gaseous phases. Nevertheless, one can assume that ultrasonic waves should have a wavelength that is much larger than the particle size.

Wavelength of p-waves in a continuum is defined as $\lambda = V_p/f$, where V_p is p-wave velocity and f is frequency. For a given f and V_p, a limiting internal scale can be established for the soil. For example, consider an ultrasonic wave with f=100kHz, and a soil from Fig. 1 with V_s=200m/s. For S=1, V_p=2000m/s and the corresponding wavelength is 20mm. For S=0.99, V_p=400m/s and the corresponding wavelength is 4mm. Grain scattering would be more likely to effect the shorter wavelengths, hence soil of a given grain size may transmit ultrasonic waves when S=1.0, but may scatter ultrasonic waves of the same frequency when S=0.99 or less. For unsaturated soils, the size of the air bubbles also constitutes an internal scale of the soil and could cause scattering due to the Brillouin effect.

Coupling

Couplants are often utilized in non-destructive testing to provide good contact between the transducer and the medium. For example, gel is used in medical ultrasound to prevent gaps between the transducer and the patient's skin that could reflect the waves back into the transducer rather than propagating the waves into the patient's body. The effect of coupling is more difficult to quantify than the effects of geometric and material damping, unsaturation, and grain scattering. Furthermore, coupling is the most common cause of poor ultrasound performance (Thomas Eischeid, Ultran Group, personal communication). In general, the authors have found that ultrasonic transducers couple better with soft soils that can conform to the shape of the surface of the transducer or delay line, and coupling improves as normal stress increases between the soil and the face of the ultrasonic transducer. At low confining stress

the ultrasonic transducers can couple well with saturated clay since tensile water pressures tend to increase normal stress even without an externally applied force. However, large normal stresses were sometimes required between the transducers and saturated sands to provide adequate coupling. For the field application discussed in this paper, large normal stresses are anticipated since the probe is pushed downward into the soil. However, stiff soils may also crack as the probe is pushed, thereby degrading coupling.

System Components

The system components for the field work performed as part of this study include the *nees@UCLA* CPT truck, transducers, source pulser, miniature DC to DC converter, receiver amplifier, receiver analog filter, rotary event-marker and proximity sensor, terminal block (SCC-68), data acquisition cards mounted in a National Instruments PXIe chassis, and a personal computer. A custom steel housing was machined to contain the transducers, pulser, DC to DC converter, and amplifier (together, these components are hereafter called the ultrasound probe). The ultrasound probe was welded to a connector rod which integrates with the existing cone penetrometer rods in the *nees@UCLA* CPT truck, permitting the ultrasound probe to be pushed vertically into the ground. The setup is schematically illustrated in Fig. 4 and shows command chain flow as well as the resulting data acquisition flow.

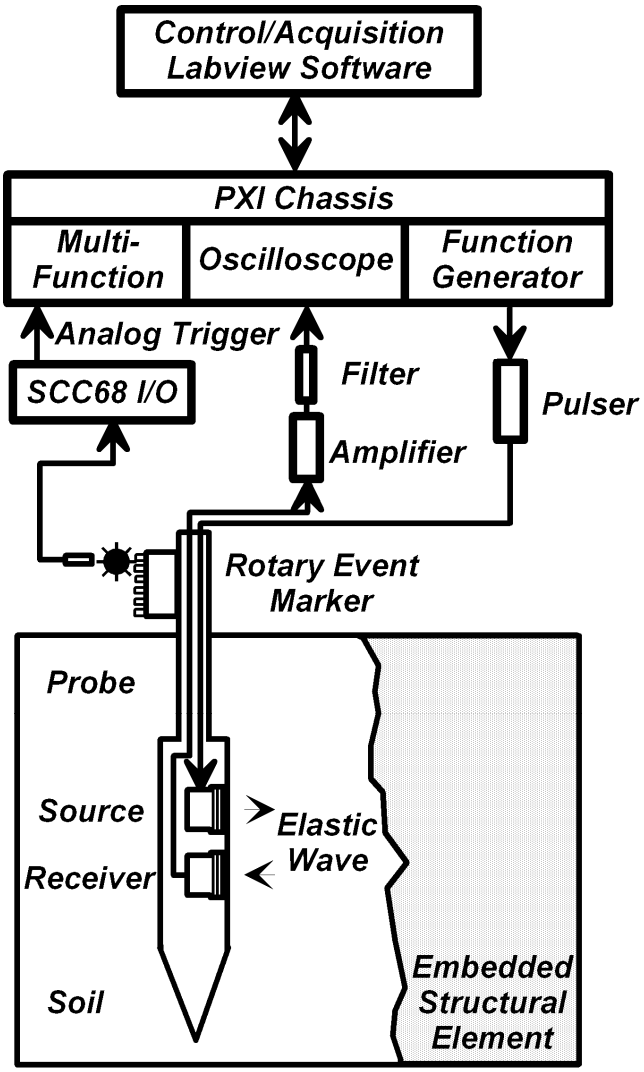

Figure 4. Schematic of probe, control system, and data acquisition system.

Ultrasonic Transducers

A set of gas matrix piezoelectric composite ultrasonic transducers manufactured by Ultran Group (State College, PA) that operate at a central frequency of 100 kHz was utilized in this study (Table 1). The transducers are composed of a gas matrix piezoelectric composite disc-shaped element, matching layer, and an insulating casing. Gas matrix piezoelectric composite

disks have inherently high damping and generate short duration pulses even without a backing block, which is often used for typical piezo materials. Short pulse durations (from highly damped transducers) are desired for pulse-echo imaging applications because "spiky" signals provide better image quality than "ringy" signals. The casing grounds the transducer and electrically shields the piezoelectric disks.

Table 1: Specifications of ultrasonic transducers.

Property	Value
Nominal Frequency	100 kHz
Manufacturer	The Ultran Group
Product No.	GRD100-D50
Length	43 mm
Diameter	50 mm

Source Pulser & DC to DC Converter

A high speed pulser provided a +150 V_{DC} input signal to the source transducer (Table 2). The pulser utilized a dual channel metal-oxide-semiconductor field-effect transistor integrated chip driver to power transducers for medical ultrasound or other applications requiring a high output current for a capacitive load. A high voltage pulse was desired to maximize the pulse amplitude to improve penetration depth and signal-to-noise ratio. A miniature DC to DC converter supplies +150 V_{DC} to the pulser, and the pulser is triggered by a 0 to +5 V_{DC} step function from an arbitrary waveform generator. The pulser outputs a step function to the transducer, which subsequently responds predominantly at its central frequency (i.e., the pulser does not permit tuning the excitation frequency). Specifications of the DC to DC converter are presented in Table 2. The converter receives a +15 V_{DC} power supply input and

converts it to a +150 V_{DC} output to provide the necessary high voltage for the source pulser to drive the piezoelectric transducers.

Table 2: Specifications of source pulser and miniature DC to DC converter.

Property	Value	Value
Manufacturer	Supertex, Inc.	EMCO
Product No.	MD1213DB1	G02
Positive Drive Voltage	10V DC	15V DC
High Voltage Supply	150V DC	N/A
Output Voltage	150V DC	150V DC
Logic Input Function	Square Waveform 0 to 5V DC amplitude	N/A
Ripple	N/A	< 0.75%

Receiver Amplifier & Filter

An inline amplifier and analog filter from the laboratory system were utilized in the field to record the voltage signal from the receiver transducer (Table 3). The amplifier was located near the receiver transducer in the steel housing to minimize cable length for the unamplified signal thereby reducing noise and minimizing loss of charge in the cable for the capacitive transducer. The amplified signal was subsequently filtered using a low-pass anti-aliasing filter with corner frequency of 2.5 MHz.

Table 3: Specifications of receiver amplifier and filter.

Property	Value	Value
Component	Amplifier	Filter
Manufacturer	Mini-Circuits	Mini-Circuits
Product No.	ZFL-500LN	BLP-1.9
Input Power	15V DC	N/A
Pass Band	0.1 to 500 MHz	N/A
Low Pass Corner Frequency	N/A	2.5 MHz
Gain	24 dB Min	N/A

Ultrasound Probe Steel Housing

A custom stainless steel housing was machined for the transducers and associated electronic hardware (Fig. 5). The housing cross section was 102×52 mm (2×4 inch) and held the transducers in contact with polypropylene delay lines that are impedance matched to saturated soil. These delay lines were in direct contact with the surrounding soil when the probe was in the ground. A thin rubber gasket and o-rings were utilized to provide a water-resistant seal for all inboard electronics. A schematic close-up of the transducers is provided in Fig. 6, which illustrates the water-resistant seal. The top of the stainless steel housing was welded to a connector rod that mates with the CPT rods onboard the 20-ton *nees@UCLA* Hogentogler CPT rig. Additionally, the same electrical connector used in the seismic piezocone was utilized in the ultrasonic probe to integrate with the cabling already threaded through the CPT rods. The steel housing facilitated quick substitution of the ultrasound probe in place of the seismic piezocone while the truck was still aligned over the hole left by the CPT sounding so that the ultrasound probe could be pushed into the same hole.

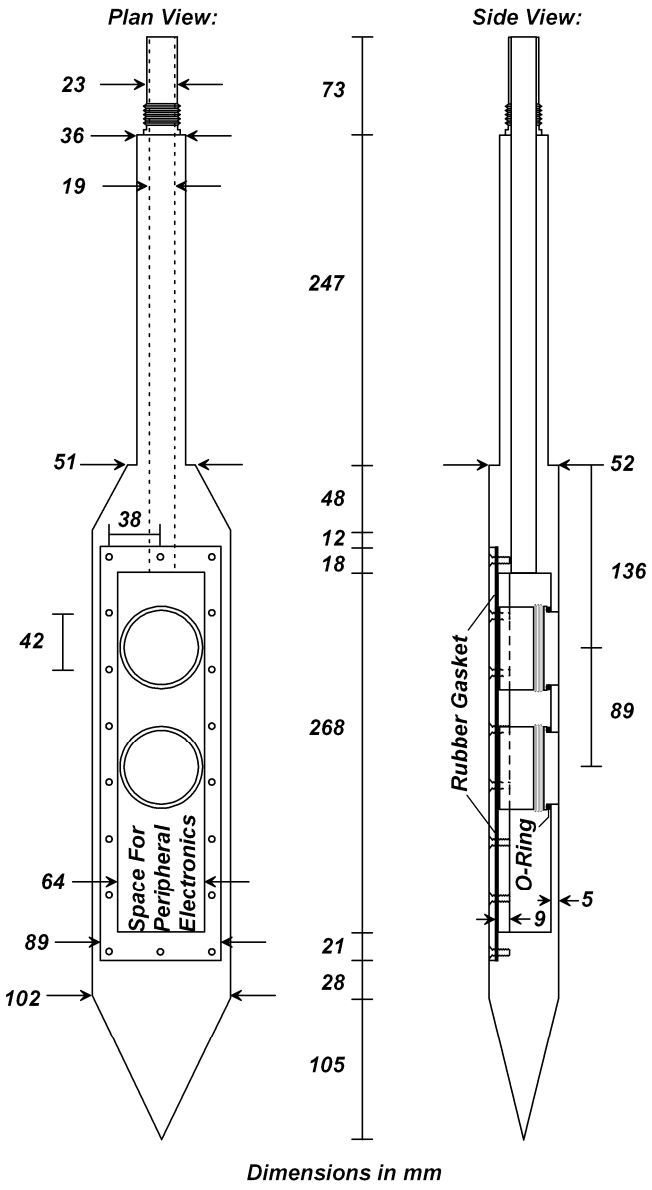

Figure 5. Detail drawing of probe.

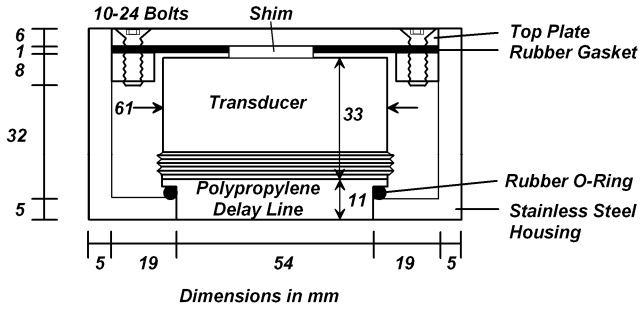

Figure 6. Close-up view of transducer inside probe.

Rotary Event Marker & Proximity Sensor

A rotary event-marker on the CPT rig measured the vertical position of the probe, and was used to trigger pulses at specified positions as the ultrasound probe was pushed in the ground. This system consisted of a 20-tooth gear with pitch diameter of 31 mm and a corresponding DC inductive proximity sensor. Specifications of the proximity sensor are listed in Table 4. The gear spun on a rack attached to the loading frame. As the ultrasound probe was pushed in the ground, the proximity sensor would trigger in response to particular gear teeth. The corresponding triggering interval was 5 cm.

Table 4: Specifications of inductive proximity sensor.

Property	Value
Manufacturer	PepperL+Fuchs
Product No.	NJ 1.5-8GM40-E-V1
Diameter	8 mm
Range	1.5 mm
Input & Output Voltage	12V DC
Switching Frequency	5 kHz

Computer Hardware & Software

Data acquisition in the field was controlled by National Instruments cards mounted in a PXIe chassis (NI-PXIe-1062Q) connected to a personal computer running custom *Labview* software (National Instruments, Austin, TX). The pulser was triggered by an arbitrary waveform generator card (NI PXI-5412), and the receiver was sampled at 5 MHz by a high speed digitizer card (NI PXI-5620). The output from the gear-tooth proximity sensor was connected to a NI SCC-68 terminal block expansion slot and sampled using a multi-function card (NI PXI-6259). These three cards were synchronized through the internal clock of the PXIe chassis.

Custom *Labview* software was written to trigger the ultrasound probe based on readings from the gear-tooth proximity sensor. The recorded pulses were saved at each specified trigger point, and metadata containing the sampling frequency, trigger points, and other salient information was written as a header and appended to the recorded voltage vectors. A single recorded pulse for the 100 kHz transducers exhibited low signal-to-noise ratio, so signal stacking was utilized to improve signal quality. An automated stacking algorithm excited a rapid succession of 75 pulses with systematically varying time intervals between pulses was used to reduce the amount of time required to perform the stacking (Brandenberg et al. 2008). Rapid stacking was needed to maintain a reasonably push rate of 2 cm/s.

Field Deployment at Carquinez Bridge Site

Site Description

The Carquinez Bridge consists of two parallel bridges which cross the Carquinez Strait linking Vallejo, California to the north, with Crockett, California to the south (Fig. 7). The site where the ultrasound testing was performed is located directly beneath the western suspension bridge span at Bent 7 adjacent to the southern anchorage. Bent 7 consists of two rectangular reinforced concrete columns approximately 3.6 m by 2.4 m in size each supported on a group of thirty-two 0.75m diameter cast-in-steel-shell (CISS) piles (NPS 30 by 0.75 steel) arranged in a 4 by 8 group configuration (Fig. 8). The pile groups are connected by a single 1.7m thick reinforced concrete pile cap with plan dimensions of approximately 30.7m by 7.2m. The center-to-center spacing between the CISS piles is 1.8 m. The CISS piles were constructed by driving steel pile casings (0.75 m diameter) to the design tip depths of approximately 41 m,

excavating the soil inside the casing, lowering steel reinforcement cages, and filling the casings with concrete. The casings were left in place and form part of the deep foundation elements.

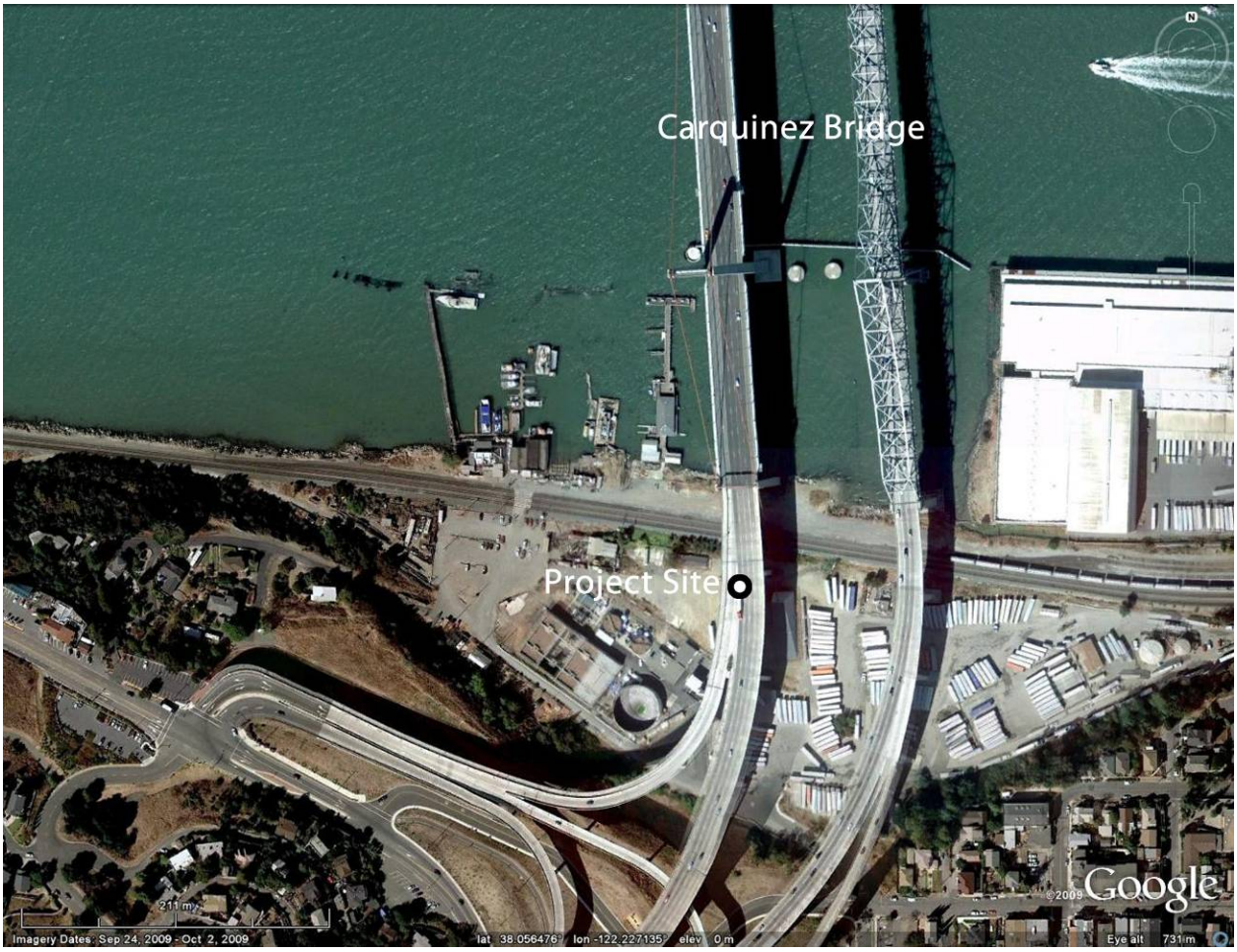

Figure 7. Image of project site at Carquinez bridge in northern California.

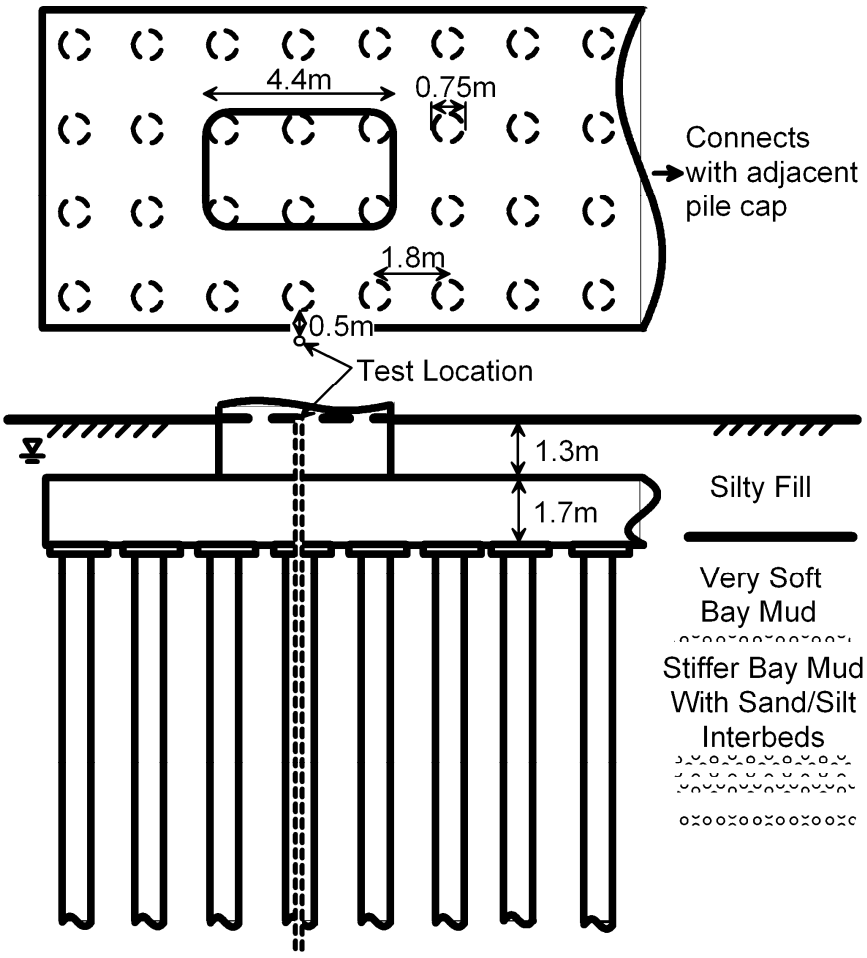

Figure 8. Schematic of bridge foundation and cone penetrometer soundings at Carquinez bridge site. Some piles are omitted for clarity.

Cone penetration soundings were performed to a depth of approximately 19m at the site (Fig. 9), and as-built drawings contained boring logs (not performed as part of this study). Soil conditions consist of approximately 2.7 m of silty fill overlying approximately 3 m of very soft bay mud over slightly stiffer bay mud with interbedded lenses of sands, silts and gravels. At a depth of approximately 23m, the bay mud is underlain by layers of siltstone, sandstone, and claystone progressing downward from weathered to competent. The depth to groundwater at this site is approximately 1.1 m. The very soft clay between depths of 3 and 5m stuck to the

CPT rods and was very messy to work with. Undrained shear strength of the clay layers was correlated with cone tip resistance, as shown in Fig. 9. A prediction based on strength normalization concepts (Ladd 1991) is also plotted in Fig. 9 for normally consolidated conditions with $s_u/\sigma_v' = 0.22$. The measured undrained shear strength is less than the normally consolidated predicted strength, which indicates that this soil is very weak and may still be consolidating under the fill. Consolidation tests were not performed to verify this evidence, but the very soft, weak consistency of the clay and low cone tip resistance are both consistent with under-consolidated conditions.

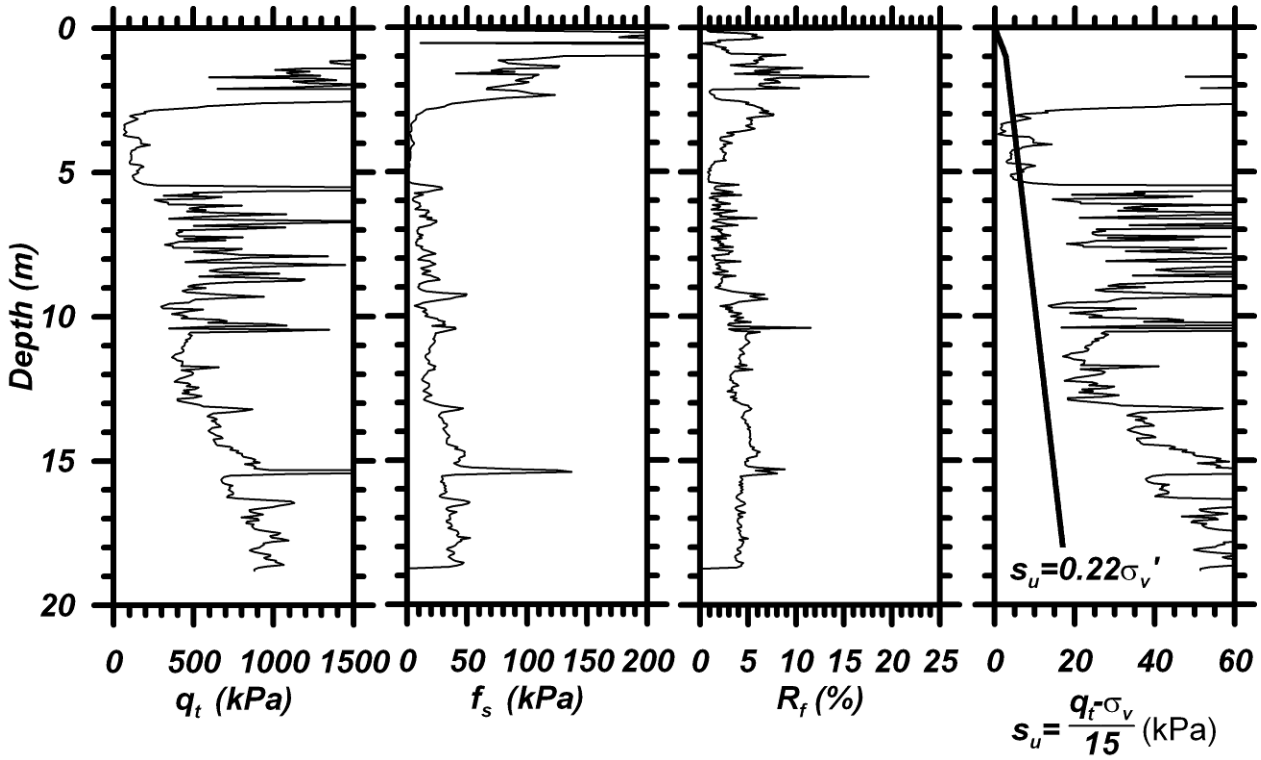

Figure 9. Cone penetration test results for Sounding No. 5 at Carquinez bridge site.

The seismic piezocone was utilized to make downhole shear wave velocity measurements (Fig. 10). The average shear wave velocity was about 310m/s in the fill layer, about 80m/s in

the soft clay layer, and about 125m/s in the underlying bay mud. The low shear wave velocity in the soft clay layer is consistent with the low tip resistance and observed consistency of the soil that stuck to the CPT rods.

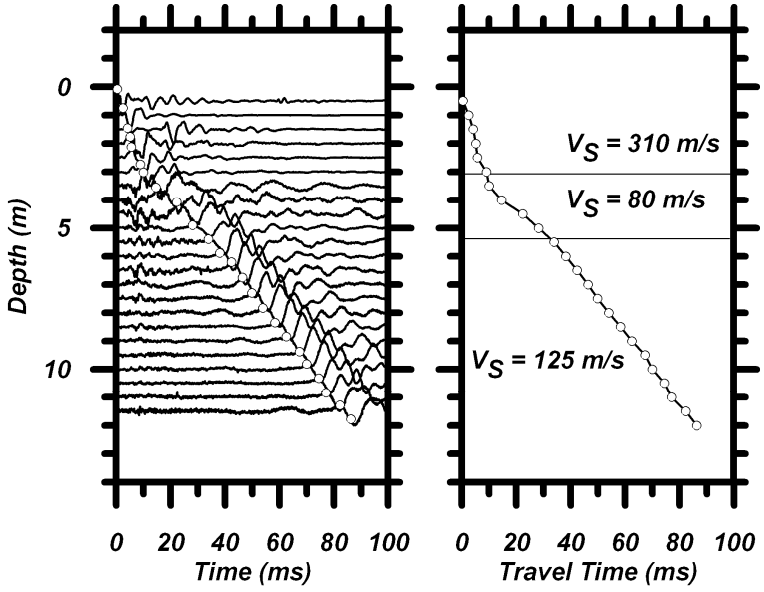

Figure 10. Shear wave velocity profile from SCPT test at Carquinez bridge site.

Ultrasound Test Results

After the CPT test was completed, the seismic piezocone was replaced by the ultrasound probe, which was pushed into the same hole to image one of the CISS piles supporting the bridge. The distance between the ultrasound probe and the pile cap was 0.1m, and the distance to the CISS pile was approximately 0.5m. The ultrasound transducers were triggered at 0.05m intervals of depth, and the recorded reflections are shown in Fig. 11. Reflections are clearly visible between depths of approximately 3 and 5 m, in the region where the transducers were in contact with the very soft bay mud. An image was constructed from the recorded voltage values by (1) mapping the recorded voltage amplitude to an 8-bit grayscale image, and

(2) computing distance between the ultrasound probe and the CISS pile by multiplying the time vector by $V_p/2$, where V_p=1460m/s was selected for saturated clay with V_s=80m/s using Eq. 2. Note that the travel times are associated with a 2-way travel path from the transducers to the pile and back, hence the need to divide by 2 to obtain one-way travel distance. The resulting image is superposed on an interpretation of the as-built sketch of the pile foundation in which the pile is assumed vertical.

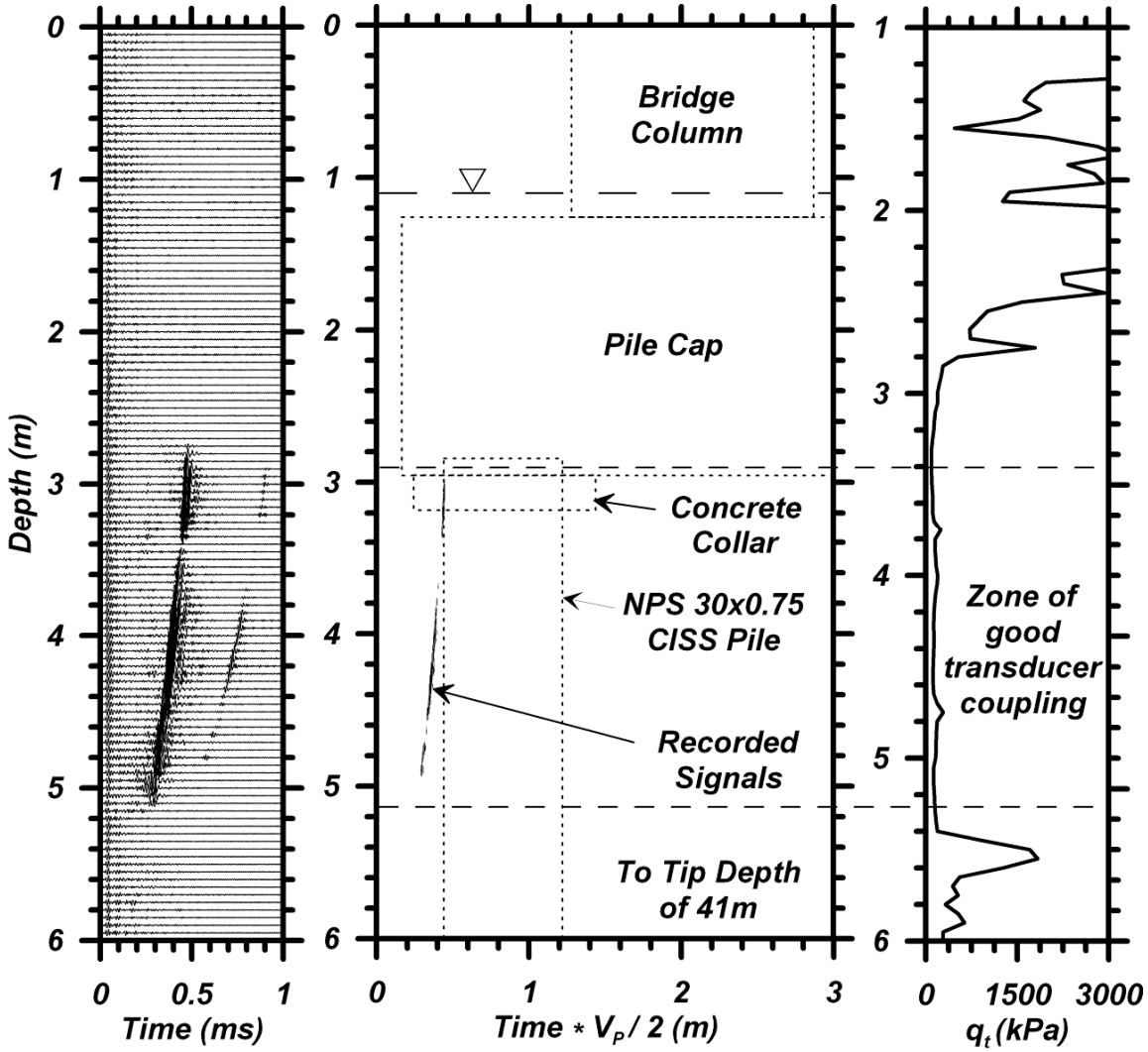

Figure 11. Recorded signals and ultrasonic image superposed on bridge sketch for Carquinez bridge site.

The travel time recorded at a depth of 3m immediately below the pile cap was approximately 0.5ms, which corresponds to an interpreted distance of ($5x10^{-4}$s*1460m/s)/2 = 0.4m. This places the reflection very close to the anticipated position of the CISS pile. However, travel time decreases as depth increases becoming as small as 2.5ms at a depth of 5m, which implies a difference in separation distance of about 0.2m. The following factors are possible explanations: (1) the CISS pile is slightly inclined away from the center of the pile group, and/or (2) the probe drifted toward the CISS pile as it was pushed, and/or (3) the p-wave velocity of the soil increased with depth. Regarding possible explanation (3), the shear-wave velocity does increase about from about 70 to 100m/s between 3-5m, but this moderate change in s-wave velocity has only a small influence on p-wave velocity, predicted to be 1461 and 1467 m/s, respectively using Eq. 2. This difference in p-wave velocity would account for only about 0.0007m of erroneous drift, which is far too small to explain the measured drift of about 0.2m. Explanation (2) could not be directly verified since the ultrasound probe was not equipped with an inclinometer (plans are in place to add this feature to the probe). However, it is likely that the probe followed the pilot hole left behind by the seismic piezocone that was equipped with a bi-axial tilt indicator, hence some knowledge of the amount of drift of the ultrasound probe can be inferred. Fig. 12 shows the recorded drift angles versus depth recorded from the seismic piezocone, and an envelope of possible sensor position obtained by integrating the vector sum of the recorded drift values versus depth. Unfortunately the orientation of the inclinometers in the CPT probe is not known, hence the probe position can only be bound by the envelope. At a depth of 5m, the drift amplitude was less than 0.1m. Even if the probe drifted directly toward the CISS pile, this amount of drift is insufficient to fully

explain the measured 0.2m separation. Hence, the measured separation distance is caused, at least in part, by drift of the CISS pile. Drift ratios as high as 10% are common for driven steel casings (Poulos and Davis 1980), and 10% drift could explain the measurements.

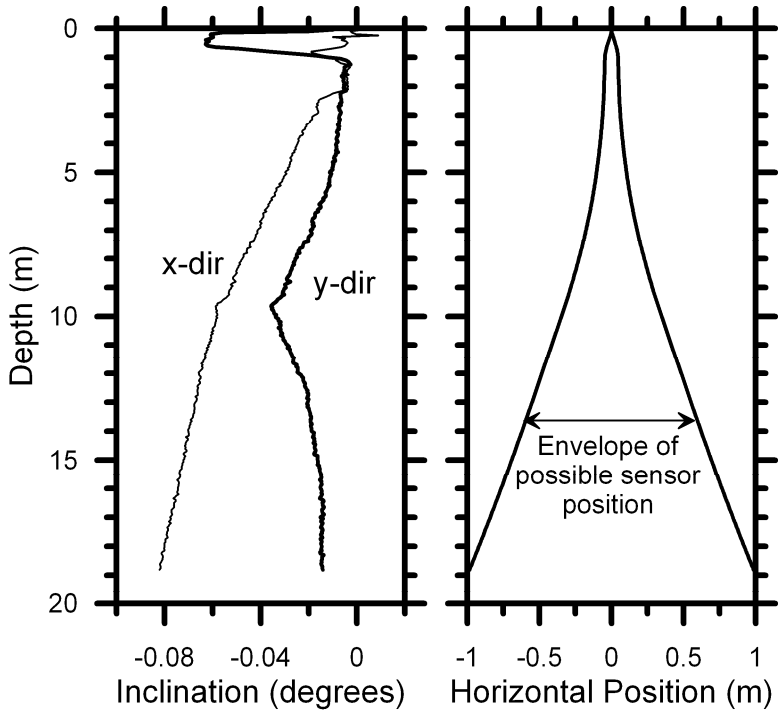

Figure 12. Cone penetrometer inclination and envelope of possible sensor position.

Returns were not recorded from reflections off of the pile cap above a depth of 3m, or from reflections deeper than about 5m in the stiffer bay mud. The fill material in contact with the pile cap was unsaturated, and this soil likely did not couple well with the transducers. Regarding the deeper bay mud, the two most likely explanations for the lack of recorded reflections are (1) the transducers did not couple well with the stiffer soils, and/or (2) the probe drifted out of alignment with the CISS pile. CPT tip resistance increases significantly below a

depth of about 5m, and this stiffer material may form cracks and imperfections that prevent adequate coupling between the transducers and the soil. However, returns were also not observed below a depth of 10m, where the tip resistance becomes smaller again. Based on Fig. 11, the probe would be expected to either hit the CISS pile at a depth of about 6 m, or drift horizontally away from the pile to avoid direct contact. There was no evidence that the seismic piezocone or the ultrasound probe made contact with the pile, hence we infer that the probe drifted laterally out of alignment with the pile. At a depth of about 10m, drift amplitude is larger than the radius of the CISS pile. This amount of drift is likely to cause significant enough misalignment between the probe and pile to prevent reflections from being recorded. Hence, it is impossible to know whether the transducers coupled well with the clay soil below a depth of 5m.

Southern California Caltrans Test Site

The field p-wave imaging system was deployed at a Caltrans-owned test site located in Hawthorne, California near the intersection of Interstate Highways 105 and 405 (Fig. 13). This site had been previously utilized by *nees@UCLA* researchers to perform load testing of full-scale drilled shafts in the field (e.g., Janoyan et al. 2006, Lemnitzer et al. 2010). This site was selected since it was close to UCLA, easily accessible, soil conditions were well-characterized by previous research studies, and contained pile foundations that could potentially be imaged. The site consists of fill overlying stiff unsaturated sandy clay, silts and sands, and the soil conditions are therefore not well-suited for coupling with the ultrasound transducers. Nevertheless, the first test using the probe was conducted at this site to verify proper integration with the CPT rig and

identify adjustments that would be required for future field studies. A particular concern was whether the probe could be pushed through stiff soils since its cross-sectional area is quite a bit larger than the seismic piezocone.

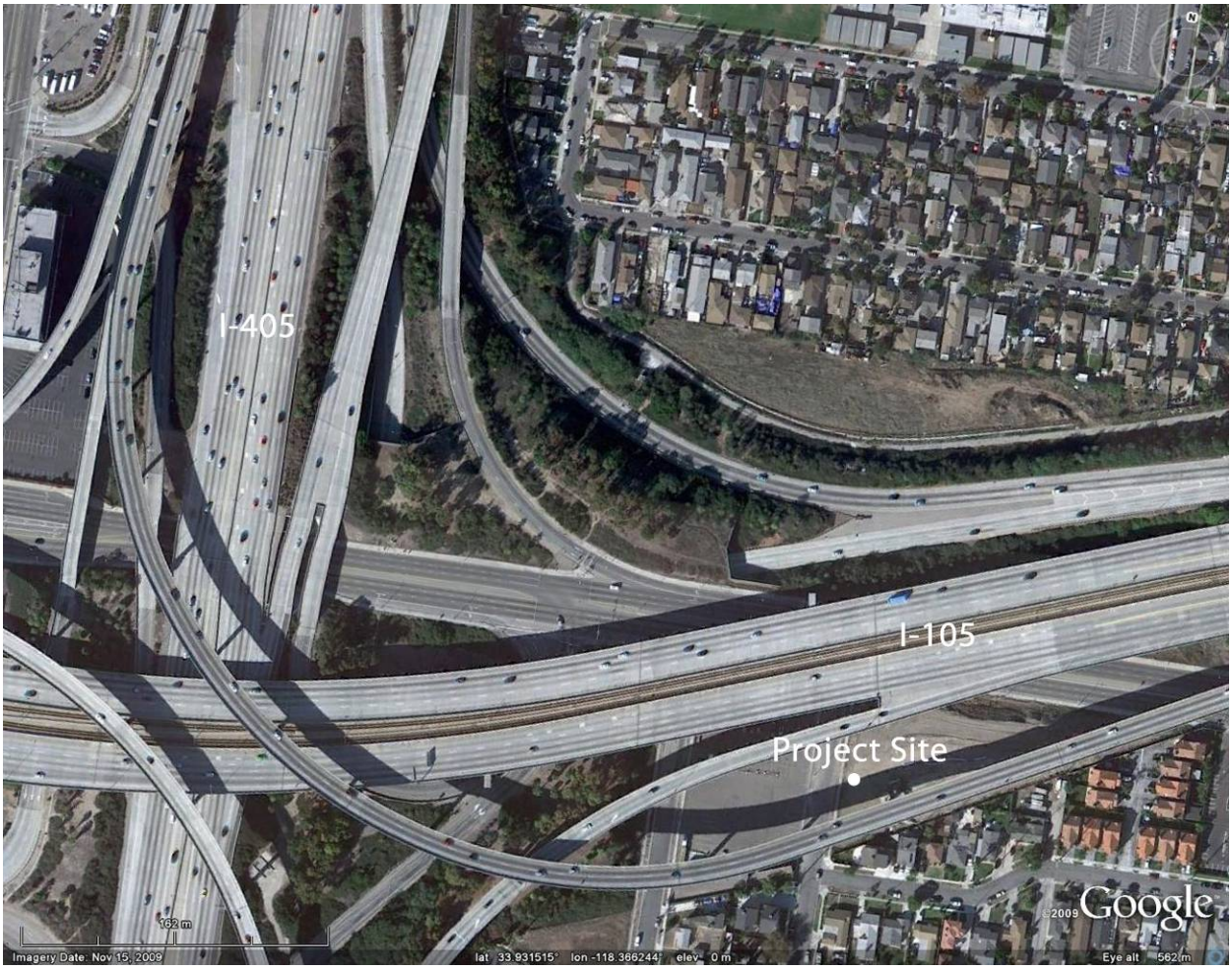

Figure 13. Southern California test site.

The deep foundations at the test site were constructed to investigate the soil-structure interaction effects of bridge support structures (e.g., Lemnitzer et al. 2010). A pile group at the site consists of nine 0.6 m diameter cast in drilled hole (CIDH) piles arranged in a 3 by 3 group configuration and a single 1.8 m thick reinforced concrete pile cap (Fig. 14). The center-to-

center spacing between the CIDH piles is 1.8 m and the pile cap has a footprint of approximately 5.4 m by 4.8 m. The CIDH piles were constructed by boring a 0.6 m diameter hole to a depth of 7.6 m, lowering steel reinforcing cages, and filling the holes with concrete.

Field testing at the site consisted of CPT data logging and p-wave imaging at two locations immediately adjacent to the CIDH pile foundation (Fig. 14). The cone penetrometer was first pushed into the ground to create a pilot hole for the ultrasound probe and to verify soil conditions against the boring logs from previous site investigations. Fig. 15 shows the cone penetration test data. The cone penetrometer was retrieved and subsequently replaced by the ultrasound probe. The ultrasound probe was then pushed into the hole left behind to facilitate penetration. As the probe was pushed alongside the CIDH piles, p-waves were emitted and the reflected energy was measured at an interval of 5 cm. However, reflections were never recorded at this site, most likely due to poor coupling between the stiff unsaturated soil and the transducers.

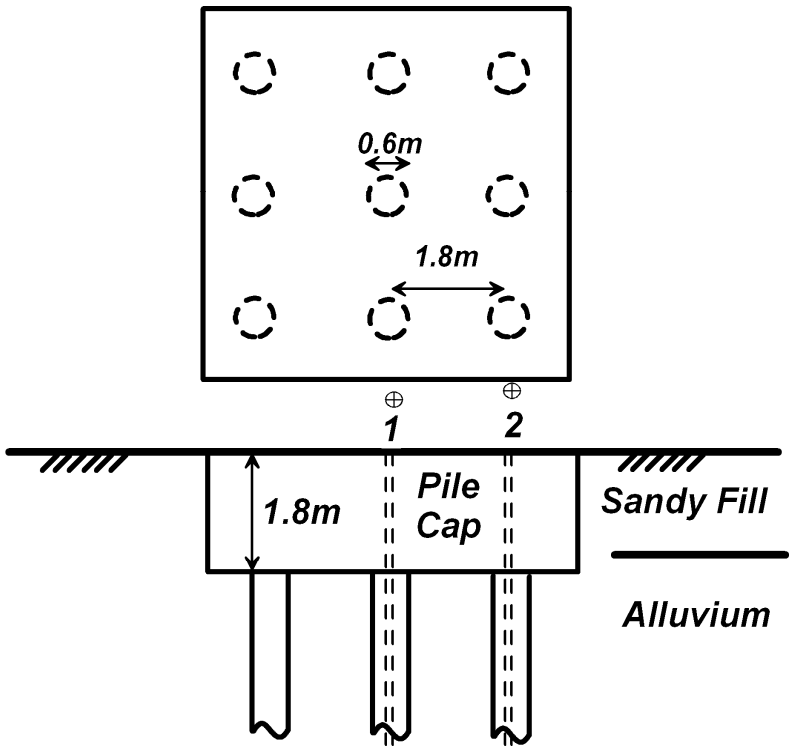

Figure 14. Schematic of pile group and location of CPT soundings at southern California test site.

While this site did not provide useful ultrasound data, it clearly establishes that the probe is not well-suited for testing stiff unsaturated soils. Additional work is needed to develop a coupling system that may permit transmission of ultrasound waves into such soil. Furthermore, the test proved useful for establishing an upper bound for the strength of soil through which the rather bulky probe can be pushed. In its first test, the ultrasound probe was pushed to a depth of only 2m and retrieved because we were concerned that difficulty might be encountered when the probe is lifted back up out of the ground and we wanted to be able to retrieve it using shovels if necessary. In the second test, the probe was pushed to a depth of 4m, where the cone tip resistance indicates the presence of a very stiff layer with q_t=35MPa.

When the probe contacted this layer, the CPT rig was lifted off of the ground, causing two of the CPT rods to be damaged due to buckling. The rods were removed and the probe was subsequently retrieved by the truck. The side augers were not in place during the test. An automated system shuts off the hydraulic pump when the seismic piezocone encounters a layer that is too stiff to push through, but the shut off is based on measurement of tip resistance, which was not present with the ultrasound probe in place. The problem encountered at the southern California test site indicates that the nees@UCLA CPT rig should not be used to push the ultrasound probe through soil with tip resistance higher than 35MPa. At the Carquinez bridge site, the probe was successfully pushed through a layer with q_t = 20MPa.

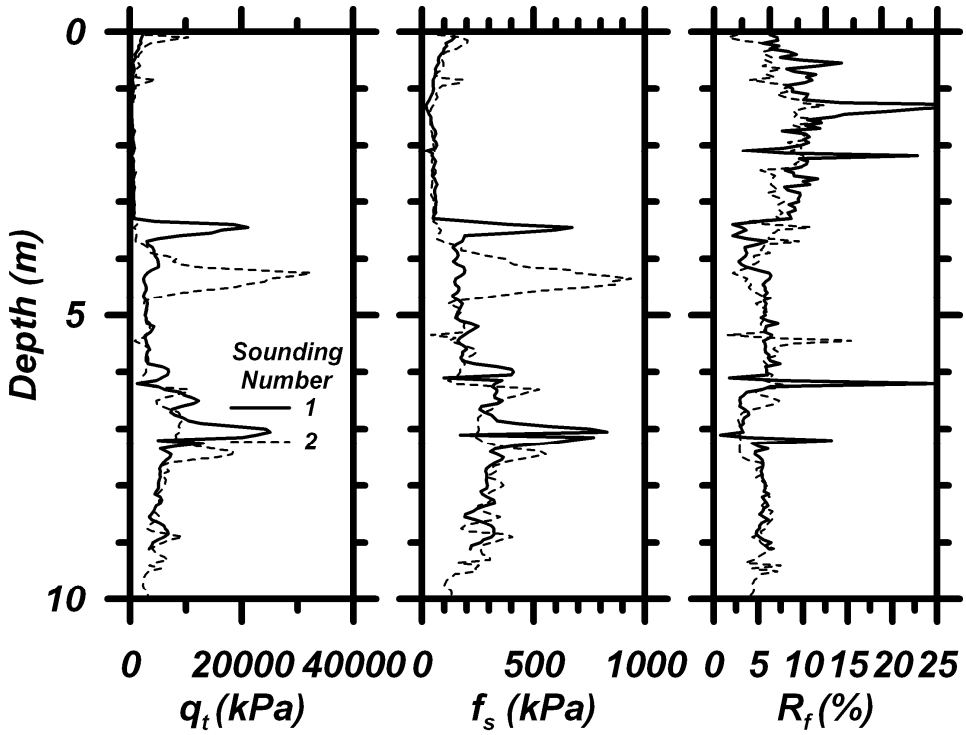

Figure 15. Results from CPT soundings at southern California test site.

CONCLUSIONS

A CPT-based ultrasonic p-wave reflection imaging system was designed, constructed, and applied in the field to image deep foundations. The probe successfully measured reflections of p-waves in very soft saturated clay. This finding is significant because the ultrasonic waves utilized in this study provide better resolution than commonly-applied geophysical methods, and image the outside of the embedded structural element, which is often a key concern. Widely utilized in other fields such as medicine and oil exploration, p-wave reflection imaging has tremendous potential to improve quality assurance in geotechnical applications. Hence, this paper is a useful contribution to a very promising neglected technology. However, the probe presented herein is not perfect, and did not provide useful measurements in stiffer and/or unsaturated soil. Probable causes of poor performance are (1) poor coupling between the transducers and the soil, (2) reduction in transmission coefficient between the transducer and unsaturated soil, and (3) drift of the ultrasonic probe away from the pile foundation. Additional research will be required to solve these problems to make the probe useful for applications over a broader range of soil conditions.

The probe, as configured, is well-suited for imaging the geometry of vertically-oriented objects embedded in very soft saturated soils. Often, structural elements are constructed in-situ in such soil conditions, and cannot be visually inspected after construction for quality assurance. A common concern for drilled shafts in soft saturated soils is that the hole may cave or squeeze prior to or during concrete placement, thereby reducing the diameter of the drilled shaft and compromising its structural integrity. Commonly-used non-destructive methods often have difficulty identifying defects along the perimeter of a structural element because (1)

methods that propagate waves from the top of the structural element have poor resolution and cannot define the shape of the anomaly, and (2) methods in which sensors are lowered into a casing constructed inside the structural element can only define properties in a small region around the casing (e.g., gamma-gamma logging), or in the region between the casings but not the perimeter (e.g., cross-hole tomography). Ultrasonic testing, when combined with these existing non-destructive techniques, has the potential to provide a more complete understanding of the properties of the structural element. Furthermore, the ultrasonic probe could be a useful quality assurance tool in many ground modification applications such as jet grouting.

Acknowledgments

The authors would like to thank Bill Owen and Yue Wu from Caltrans for providing resources and technical oversight during the field explorations at the Carquinez Bridge site. Assistance by the nees@UCLA staff, particularly Robert Nigbor and Alberto Salamanca, is also gratefully acknowledged. Funding for this work was provided by UCLA and by Caltrans under contract number 59A0691. The cone penetration testing (CPT) truck was utilized in collaboration with the nees@UCLA equipment site which is funded by the George E. Brown, Jr. Network for Earthquake Engineering Simulation (NEES) established by the National Science Foundation (NSF). The contents of this report reflect the views of the authors who are responsible for the facts and accuracy of the data presented herein. The contents do not necessarily reflect the official views or policies of the State of California or the Federal Highway Administration. This report does not constitute a standard, specification, or regulation.

References

Berge, P.A., and Bonner, B.P. (2002). "Seismic velocities contain information about depth, lithology, fluid content, and microstructure." *Symposium on the Application of Geophysics to Engineering and Environmental Problems*, Los Vegas, NV, Feb. 10-14, 2002.

Biot, M., (1956a) "Theory of propagation of elastic waves in fluid-saturated porous solid. I Low frequency range." *J. Acoustical Society of America*, 28, 168-178.

Biot, M. (1956b). "Theory of propagation of elastic waves in fluid-saturated porous solid. II. High frequency range." *J. Acoustical Society of America*, 28, 179-191.

Brandenberg, S. J., Kutter, B. L., and Wilson, D. W. (2008). "Fast Stacking and Phase Corrections of Shear Wave Signals in a Noisy Environment." *J. Geotech. Geoenviron. Eng.*, 134(8), 1154-1165.

Brillouin, L. (1946). "Wave propagation in periodic structures." *McGraw Hill*, *New York,* 247p.

Coe, J. T. and Brandenberg, S. J. (2010). Accepted for Publication. "P-wave Reflection Imaging of Submerged Soil Models Using Ultrasound." *J. Geotech. Geoenviron. Eng.*

Cormack, A.M. (1963). "Representation of a function by its line integrals, with some radiological applications." *J. Appl. Physics.* No. 34. pp. 2722-2727.

Doroudian, M. and Vucetic, M., (1995). "A Direct Simple Shear Device for Measuring Small-Strain Behavior," *ASTM Geotechnical Testing Journal*, Vol. 18. No. 1, pp. 69-85.

Grandjean, G. (2006). "A seismic multi-approach method for characterizing contaminated sites." *J. of Applied Geophysics*. 58. 87-98.

Hertlein, B. H., and Davis, A. G. (2006). *Nondestructive Testing of Deep Foundations*. John Wiley and Sons, Chichester, England. 270 pp.

Hounsfield, G.N. (1973). “Computerized transverse axial scanning (tomography): part 1. Description of system.” *Br. J. Radiol.* No. 46, pp. 1016-1022.

Janoyan, K. D., Wallace, J. W., and Stewart, J. P. (2006). "Full-Scale Cyclic Lateral Load Test of Reinforced Concrete Pier-Column." *American Concrete Institute Structural Journal*, 103(2), 178-187.

Kase, E.J., and Ross, T.A. (2004). "Seismic imaging to characterize subsurface ground conditions in civil construction." *Proc. Geo-Trans, 2004. ASCE Special Publication No. 126.* 1823-1831.

Ladd, C. C. (1991). “Stability Evaluation During Staged Construction: 22nd Terzaghi Lecture.” *J. Geotech. Geoenviron. Eng.*, 117(4), 540-615.

Ladd, C. C., and Foote, R. (1974). “A New Design Procedure for Stability of Soft Clays.” *J. Geotech. Eng. Div.*, 100(GT7), 763-786.

Lee, J. S. (2003). “High Resolution Geophysical Techniques for Small-Scale Soil Model Testing.” Ph.D. dissertation. Georgia Institute of Technology, Atlanta.

Lee, J. S., and Santamarina, J. C. (2005). “P-Wave Reflection Imaging.” *Geotech. Test. J.*, 28(2), 197-206.

Leedom, D.A., Krimholtz, R., adn Matthaei, G.L. (1971). "Equivalent circuits for transducers having arbitrary even- or odd-symmetry piezoelectric excitation." *IEEE Transactions on Sonics and Ultrasonics*. SU-18(3), 128-141.

Lemnitzer, A., Khalili-Tehrani, P., Ahlberg, E. R., Rha, C., Taciroglu, E., Wallace, J. W., and Stewart, J. P. (2010). Accepted for Publication. “Nonlinear Efficiency of Bored Pile Group Under Lateral Loading.” *J. Geotech. Geoenviron. Eng.*

Lunne, T., Robertson, P. K., and Powell, J. J. M. (2002). *Cone Penetration Testing in Geotechnical Practice*. Spon Press, London, England. 312 pp.

Mohorovičić (1910). *Jb. Meteorol. Obs. Zagreb, fur 7909* Bd. 4, Teil 4, Ab. 1.

Naesgaard, E., Byrne, P.M., and Wijewickreme, D. (2007). "Is P-wave velocity an indicator of saturation in sand with viscous pore fluid?" *Int. J. Geomechanics.* 7(6). 437-443.

Nichols, T.C., King, K.W., Collins, D.S., and Williams, R.A. (1987). "Seismic-reflection technique used to verify shallow rebound fracture zones in the Pierre Shale of South Dakota." *Can. Geotech. J.* 25, 369-374.

Olson, L.D., and Aouad, M.F. (1998). "NCHRP 21-5 Research Results on Determiniation of Unknown Bridge Foundation Depths." *International Water Resources Engineering Conference*, Memphis, Tennessee, August 3-7, 1998.

Persson, H.W., and Hertz, C.H. (1985). "Acoustic impedance matching of medical ultrasound transducers." *Ultrasonics*. 23(2). 83-89.

Poulos, H. G., and Davis, E. H. (1980). *Pile Foundation Analysis and Design*. John Wiley and Sons, New York, NY. 397 pp.

Qiu, T. (2010). "Analytical solution for Biot flow induced damping in saturated soil during shear wave excitations." *J. Geotech. Geoenviron. Eng.*, Posted ahead of print on March 27, 2010.

Santamarina, J. C., and Fratta, D. (2005). *Discrete Signals and Inverse Problems: An Introduction for Engineers and Scientists*. John Wiley and Sons, Chichester, England. 350 pp.

Santamarina, J. C., Klein, K. A., and Fam, M. A. (2001). *Soils and Waves: Particulate Materials Behavior, Characterization and Process Monitoring*. John Wiley and Sons, Chicester, England. 488 pp.

Sheriff, R.E., and Geldart, L.P. (1995). "Exploration Seismology." *Cambridge University Press,* Cambridge, 592p.

Stokoe, K.H., II Wright, S.G., Bay, J.A. and Roesset, J.M., 1994, "Characterization of Geotechnical Sites by SASW Method," ISSMFE Technical Committee #10 for XIII ICSMFE, Geophysical Characterization of Sites, A. A. Balkema Publishers/Rotterdam & Brookfield, Netherlands, pp. 15-25.

Terzaghi, K. (1947). *Theoretical Soil Mechanics*. Fourth Printing. John Wiley and Sons, New York, NY. 510 pp.

Wallace, J. W., Fox, P. J., Stewart, J. P., Janoyan, K., Qiu, T., and Lermitte, S. (2001). "Cyclic Large Deflection Testing of Shaft Bridges. Part I: Background and Field Test Results," Civil and Environ. Eng. Dept., University of California, Los Angeles.

Yilmaz, O. (1987). *Seismic Data Processing*, Society of Exploration Geophysicists, Tulsa, OK. 526 p.